Morphological features and crystallization behavior of the conductive composites of poly(trimethylene terephthalate)/graphene nanosheets

Chien-Lin Huang, Yu-Jyun Wang, Yang-Chun Fan
Department of Fiber and Composite Materials, Feng Chia University, Taichung, 40724, Taiwan
Correspondence to: C.-L. Huang (E-mail: clhuang@mail.fcu.edu.tw)

ABSTRACT: Poly(trimethylene terephthalate) (PTT) composites filled with well-dispersed graphene nanosheets (GNSs) were prepared through a coagulation method. The effects of increased GNS concentration on variations in the structure and properties of the PTT matrix, such as its electrical conductivity, crystallization kinetics, melting behavior, and crystal morphology, were investigated. Several analytical techniques were used, including electrical conductivity measurement, differential scanning calorimetry, Fourier transform infrared spectroscopy, wide-angle X-ray diffraction, polarized light microscopy, transmission electron microscopy (TEM), and thermo-gravimetric analysis (TGA). Electrical conductivity increased from 1.8×10^{-17} S/cm for neat PTT to 0.33 ± 0.23 S/cm for PTT/GNS composites with 2.97 vol % GNS content. Percolation scaling laws were applied, and then threshold concentration and exponent were determined. In the case wherein liquid nitrogen was used to quench the melt, a mesomorphic phase was formed despite the extremely short crystallization time after adding high GNS contents. PTT crystallization rate increased with the gradual addition of GNSs. The enhanced crystallization kinetics was attributed to the high nucleation ability of GNSs to induce epitaxially grown lamellae on their surfaces, as revealed by TEM. PTT nuclei were randomly developed on the GNS surface to form the lamellae. However, crystallinity reached its maximum value near the electrical percolation threshold because the PTT chain mobility was confined after the GNS–GNS network formed. The growth of PTT banded spherulites in the bulk was still observed for composites with high GNS content, and TGA results revealed that the GNS-filled PTT composites had excellent thermal stability. © 2016 Wiley Periodicals, Inc. J. Appl. Polym. Sci. **2016**, *133*, 43419.

INTRODUCTION

Graphene nanosheets (GNSs) with thickness of several nanometers as well its related materials, such as carbon nanotubes (CNTs), are some of the most promising materials for advanced applications because of their excellent mechanical and electrical properties and large surface areas.[1] Thus, GNSs have become widely explored in various applications and have been extensively studied, particularly in the area of polymer composites.

In recent years, several studies have reported various processing routes for incorporating carbon nanofillers into polymer matrices, such as melt compounding,[2–4] *in situ* polymerization,[5,6] emulsion polymerization,[7–10] solution casting,[11] and coagulation.[12–16] In conductive application of GNS-based composites, electrical conductivity and the lowest GNS load required are important considerations. Stankovich *et al.*[13] applied a coagulation mixing method to prepare polystyrene (PS) composites filled with chemically modified GNSs and achieved an electrical percolation threshold as low as 0.1 vol %. Notably, functionalizing GNS surfaces may provide a possible route to improve GNS–polymer interactions and form good filler dispersion, but may also deteriorate the intrinsic conductivity of GNSs. Using a coagulation method without functionalizing GNS surfaces may be a reasonable route to yield a single GNS into a polymer matrix with higher electrical conductivity.[17] In our previous work,[15,18] unmodified CNTs and GNSs were properly dispersed in the syndiotactic PS (sPS) matrix through a simple coagulation process using *ortho*-dichlorobenzene (*o*-DCB) as solvent and methanol as non-solvent. Numerous studies have attempted to incorporate GNSs into polyester via melt compounding; however, only few have reported information on the incorporation of GNSs into polyester via coagulation. Moreover, preparing polyester/GNS composites using coagulation method is difficult because polyester is only soluble in strong polar solvents, such as hexafluoroisopropanol, trifluoroacetic acid, and phenol; by contrast, GNSs precipitate in polar solvents. Hu

---

et al.[16] prepared poly(ethylene terephthalate) (PET) composites filled with multi-walled carbon nanotubes (MWCNT) by employing a simple coagulation process using *o*-DCB-phenol as solvent and observed strong interaction between the PET chains and the acid-treated MWCNTs. They reported a low percolation threshold for electrical conductivity of 0.9 wt % MWCNT. Thus, a coagulation process using *o*-DCB-phenol as solvent is a promising method for preparing polyester/GNS composites.

Addition of GNSs and CNTs to semi-crystallized polymers also changes their crystalline modification, morphology, and crystallization kinetics. The crystallization of GNS-filled or CNT-filled polyethylene (PE),[19,20] isotactic polypropylene (iPP),[21,22] sPS,[23,24] PET,[4] polylactide,[25,26] and poly(trimethylene terephthalate) (PTT)[27] has been investigated. The results of these studies show that GNSs and CNTs act as effective nucleating agents and increase the overall crystallization rate by significantly enhancing heterogeneous nucleation. The crystallization of semi-crystallized polymer on a filler surface provides a potentially effective route to achieve strong polymer–filler interaction. Thus, polymer–filler interfacial crystallization can improve interfacial adhesion and reinforce composites.[28] The nucleation ability of individual CNTs and GNSs has been clearly observed through transmission electron microscopy (TEM) on the basis of solution crystallization;[19,20] that is, the nanohybrid "shish-kebab" structure has been developed, with CNTs as the "shish" decorated with the PE-crystal "kebab." The PE epitaxial crystallization on GNS surfaces though controlled solution crystallization has also been investigated. Combining TEM and differential scanning calorimetry (DSC), Lu *et al.*[21] provided the first microscopy images of CNTs nucleating iPP when crystallizing from a quiescent melt. The images showed that iPP crystals form a transcrystalline layer of aligned iPP lamella crystals around the nucleating CNT. Xu *et al.*[25] found that the strong non-covalent bond interaction between GNS and poly-L-lactide (PLLA) chains results in unique conformational order of PLLA/GNS nanocomposites; this outcome may be explained in terms of a surface-induced conformational order. According to our previous studies,[18] the nucleating ability of GNSs with wrinkled surfaces is weaker than that of GNSs with smooth surfaces. Thus, the epitaxial nucleation at GNS surfaces is dominant in the melt-crystallization of sPS/GNS composites.[18] However, data on the lamella crystal morphologies of polyester/GNS composites from the melted state are lacking.

Xin *et al.*[26] showed that GNSs function as heterogeneous nucleating agents for PLLA composite crystallization and as a confined space for PLLA crystal nucleation and growth at a formed GNS–GNS network structure. Aoyama *et al.*[4] reported the crystallization behavior of PET composites filled with GNSs. A confinement effect is required to suppress the crystallization of PET composites with increased GNS contents. The interparticle distance between PET and GNS decreases with increased GNS contents. This condition results in a geometrically restricted PET chain. Therefore, competition exists between nucleation and confinement effects during GNS-filled polymer crystallization. Nevertheless, the reason behind the decreased crystallinity of polymer/GNS composites with geometrically restricted polymer chain remains unknown.

PTT is an engineering thermoplastic with faster crystallization rate and better mechanical properties than PET and poly(butylene terephthalate), respectively. Moreover, PTT reportedly possesses the physical properties of nylons, namely, elastic recovery, good chemical resistance, and quick crystallization rate. Thus, PTT is suitable for versatile applications such as manufacture of fibers, films, and engineering thermoplastics. For melt crystallization, PTT crystallizes into a triclinic structure.[29] Recently, Chuang *et al.*[30] found that PTT enters a mesomorphic phase and nanograin development during cold crystallization. However, little information is available on the influence of GNS load on cold crystallization of PTT composites.

Xu *et al.*[31] found that the crystallization rate of PTT composites increases with gradually increased CNT content. Li *et al.*[3] investigated the non-isothermal crystallization kinetics of PTT composites using GNS as fillers. The melt crystallization temperature of PTT/GNS composites increases with increasing GNS content. Paszkiewicz *et al.*[32] found that the lamella thickness of PTT/GNS composites is almost similar to that of neat PTT during non-isothermal crystallization. Guo *et al.*[33] performed non-isothermal and isothermal DSC tests and found that the overall crystallization rate of PTT increases in the presence of graphite oxide (GO). However, the presence of GO influences spherulitic morphology by acting as a nucleating agent, although three-dimensional (3D) spherulite also occurs. Moreover, a strong interaction between PTT and GO has been observed because of the presence of hydrogen bonds between the PTT and the oxygen functional groups of GO. However, the remaining oxygen functional groups of GNS are significantly fewer than those of GO, indicating that the amount of hydrogen bonds between PTT and GNS is lower than that between PTT and GO. Although references on crystallization of PTT/GNS or PTT/GO composites are available, the differences in crystallization between PTT/GNS and PTT/GO composites remain unknown.

In the present work, PTT composites filled with well-dispersed GNSs were prepared through a coagulation method using *o*-DCB-phenol as solvent. The conductive properties and morphology of the PTT composites were investigated to determine the GNS dispersion effect. A systematic study on the effects of GNS loading on the nucleation ability, lamella morphologies, crystallinity, crystallization kinetics, melting behavior, and spherulitic morphologies of PTT composites is necessary to obtain a comprehensive understanding on manipulation of the epitaxial crystallization of PTT/GNS composites. The influence of GNS loading on the cold crystallization of PTT composites were determined by Fourier transform infrared (FTIR) and wide-angle X-ray diffraction (WAXD). The lamellar morphologies of the polymer composites filled with GNSs from melt crystallization were observed using TEM to investigate the reduced crystallinity of the semi-crystallized polymers with increased GNS contents. The association between crystallization kinetics and the GNS–GNS network of the polymer composites was also investigated.

EXPERIMENTAL

Materials and Composite Preparation

PTT was purchased from DuPont Co.; *o*-DCB was purchased from ARCOS. The molecular weight of PTT was determined

from the intrinsic viscosity $[\eta]$ of phenol/tetrachloroethane (60/40, w/w) at 30 °C[34]; that is, $[\eta] = 5.36 \times 10^{-4} M_v^{0.69}$, where M_v is the viscosity-average molecular weight. According to the plot of the reduced and inherent viscosity of PTT (Supporting Information, Figure S1), the determined M_v of PTT was 53,100 g/mol. Phenol was purchased from Showa Chemical Co.; GNSs were purchased from Angstron Materials, LCC (N002-PDR). According to the manufacturer, the average thickness of the GNSs was lower than 1 nm, relative to the three-layer graphenes. The PTT and GNSs had densities of 1.28[35] and 2.20 g/cm³, respectively.

The GNSs were added to the o-DCB-phenol (1:1, v/v) solvent, after which ultrasonic treatment was performed for 6 h. The weighed PTT pellets were then added. Afterward, the mixture, with 1% (w/v) solid content was stirred at 140 °C to dissolve the PTT pellets. The uniform suspension solution was precipitated dropwise into a 20-fold excess volume of methanol. The precipitated powders were continuously dried in a vacuum oven until the residual solvent was removed. In this work, a sample code of 99/1 denotes the weight ratio of the matrix to the filler, whereas ϕ and ϕ_{GNS} denote the GNS volume percentage and weight percentage, respectively.

Characterization

PTT/GNS composite films were prepared by hot-pressing the dried powders in rectangular steel molds (thickness: 0.3 mm) at 280 °C for 3 min, followed by air cooling to room temperature. Measurements for the samples with high electrical conductivity ($>10^{-6}$ S/cm) were performed using a Keithley 2400 source-meter. The standard four-probe technique was applied to reduce the effects of contact resistance with applied voltage between 1 and 20 V. A Keithley 6487 electrometer equipped with a Keithley 8009 resistivity fixture was used for the samples with low electrical conductivity ($<10^{-6}$ S/cm) based on the ASTM D257 standard. The applied voltage for the sample with low electrical conductivity was between 100 and 500 V.

The crystallization and melting behavior of the PTT/GNS composites were investigated using a Perkin–Elmer DSC7 under a N_2 atmosphere. Prior to the measurements, indium and zinc standards were used to calibrate the fusion enthalpies and melting temperatures. The melt-quenched samples were heated to 280 °C at 10 °C/min to perform non-isothermal crystallization for the cold crystallization study (first heating scan). After maintaining 280 °C for 10 min, the samples were cooled to room temperature at a rate of 10 °C/min for the melt crystallization study (first cooling scan).

For isothermal crystallization, the prepared composites were first held at 280 °C for 10 min, and then rapidly cooled to the desired crystallization temperature (T_c) until a complete phase transformation occurred. A subsequent heating trace was obtained at a heating rate of 10 °C/min. This process was performed to determine the melting behavior of the composites.

FTIR measurements were performed using a Perkin-Elmer FTIR spectrometer (Spectrum 100) equipped with a Mettler heating stage (FP900) for temperature control. A total of 32 scans with a 2 cm^{-1} resolution were obtained for each spectrum. The

WAXD intensity profiles of the PTT/GNS composite films were obtained using a Bruker diffractometer (NanoSTAR Universal System, Cu K$_\alpha$ radiation). A polarized light microscope (PLM, Nikon, Eclipse LV100 POL) equipped with a hot stage (THMS600, Linkam) was used to observe the PTT spherulites formed in the crystallized composites.

The dispersion of GNSs in the samples was examined with TEM (Joel JEM-2000FX) operated at 80 kV. For the composite samples, the films were prepared by sectioning bulk samples at room temperature with an Ultracut UCT (Leica) microtome, whereas ultrathin films with approximately 50 nm thickness were observed using TEM. The GNS surface was investigated via atomic force microscopy (AFM) under the tapping operation mode. AFM observations were performed at room temperature using a Nanoscope Multimode IIIa (Digital Instruments) apparatus.

Thermo-gravimetric analysis (TGA) was performed on a TGA 2050 (TA instrument) apparatus under nitrogen flow (90 mL/min) from 25 °C to 800 °C at a heating rate of 10 °C/min. The weight of the samples used was approximately 5 mg. The degradation temperature (T_d) was defined as the temperature at which the weight loss reached 5%.

RESULTS AND DISCUSSION

GNS Characterization

The GNS morphology was characterized by TEM. Figure 1(a) shows the structure of the deposited GNS on the TEM grid prepared using the o-DCB solution. The GNS structure exhibited a 1.83 μm×1.29 μm lateral dimension and was transparent with folding and wrinkling. To determine the average long and short axes of the GNSs, more than 150 measurements of the long and short axes were obtained. The number-average long and short axis lengths were 1243.6 ± 711.9 nm and 509.7 ± 282.4 nm, respectively. Figure 1(b) shows the AFM image and height profile of the GNSs. Samples were prepared by depositing a drop of the GNS/o-DCB solution onto mica, followed by drying. The thickness of the GNS for the flat regions was approximately 2.5 nm. The height analysis of the minimum GNS thickness measured on 20 different sheets yielded an average minimum GNS thickness of 3.7 ± 0.8 nm. The GNS thickness from the AFM measurements was slightly higher than that reported by the manufacturer. According to Garboczi et al.,[36] the aspect ratio can be defined as a/b, where a is the length of the symmetry axis, b is the length of each axis perpendicular to the symmetry axis, and a/b is the aspect ratio of the ellipsoid. Although the GNSs were not uniform or regular in terms of their lateral size or shape, the GNS area can be calculated by multiplying their long and short axes. b was calculated by taking the square root of the product of the long and short axes, whereas a was the average minimum GNS thickness. Consequently, the GNS aspect ratio was about 1/217.

As observed in the FTIR spectra of the GNS (Supporting Information, Figure S2), the small peaks at 1655, 1393 and 1110 cm^{-1} can be attributed to the stretching vibration from C=O, bending vibrations from O—H, and stretching vibration from C—O, respectively.[37–39] The intensities of the peaks of the
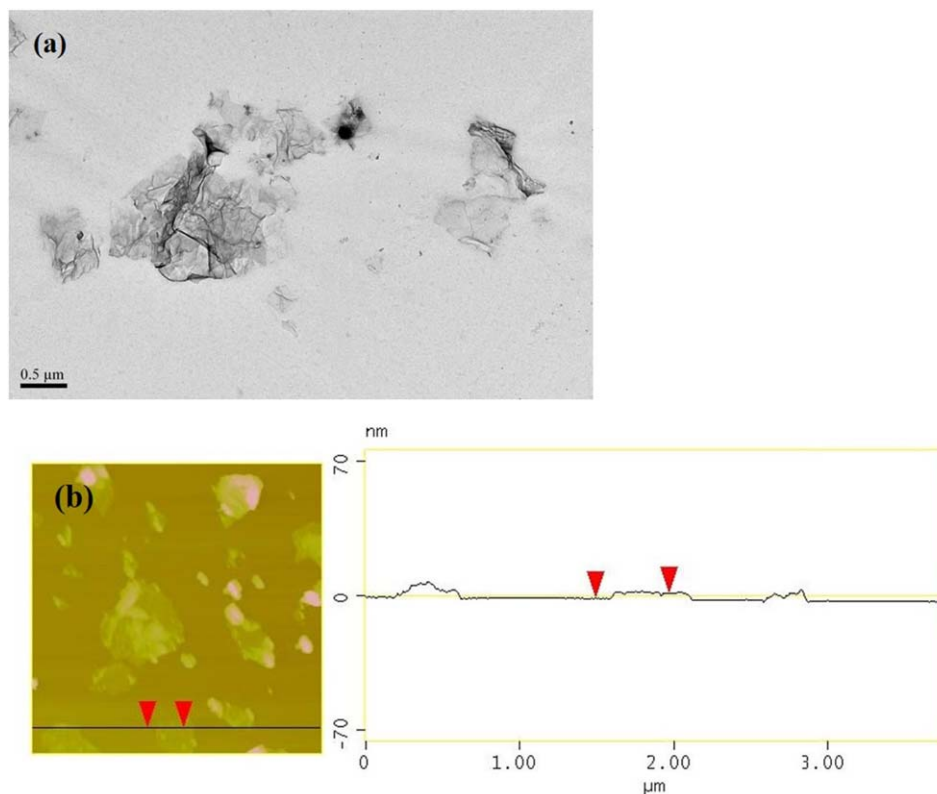
Figure 1. (a) TEM images of GNS dispersion in o-DCB solution, and (b) AFM images and corresponding height profiles of GNS. [Color figure can be viewed in the online issue, which is available at wileyonlinelibrary.com.]

GNSs associated with oxygen functional groups were extremely smaller than those of GO in our previous work.[40] As indicated in the Raman spectra in our previous study,[18] the G and D bands at 1582 and 1341 cm^{-1} of GNS nanofillers were broad. Moreover, the intensity ratio of the G/D band was approximately 0.73. Thus, GNSs possessed a few defects, which are associated with the in-plane vibration of graphene layers and the minimal number of oxygen functional groups.

Electrical Conductivity of PTT/GNS Composites

After ultrasonic treatments, nonpolar GNSs in the o-DCB solvent can exhibit uniform dispersion, whereas PTT can dissolve in phenol at high temperature but not in o-DCB solvent. Moreover, o-DCB is miscible solution with phenol. Thus, o-DCB-phenol (1:1 by volume) may be more suitable than other solvents, for producing well-dispersed GNS-filled PTT composites. The performance of polymer composites depends strongly on the state of filler dispersion in the matrix. In this work, the TEM images revealed the dispersion of GNSs on composite morphology. Figure 2 shows several typical TEM images of the PTT/GNS composites. The GNS-GNS network can be clearly observed in Figure 2(a) because the 1 wt % GNS content in the PTT composites was slightly higher than the electrical percolation threshold (ϕ_c) of the PTT/GNS composites (as discussed later). As indicated by the thin arrows in the TEM images shown in Figure 2(b), which was enlarged from Figure 2(a), some of the GNSs appeared to scroll into the tubes. This phenomenon highlighted the thin isolated GNSs heated above the polymer glass transition in the polymer/GNS composites.[41]

When the GNS content was increased to 5 wt % [Figure 2(c)], several GNSs aggregated in the PTT/GNS composites; however, the polymer areas without GNS were reduced. Under higher magnification [Figure 2(d)], a crumpled and layered stack conformation was observed in the GNSs. This result indicated that the PTT/GNS composites prepared through the solution method had a combination of exfoliated/intercalated morphologies.

Although electron microscopy may provide local information on composites, electrical conductivity data coupled with percolation laws are more appropriate for describing the global dispersion of the GNSs in solid state. The percolation threshold used to characterize the dispersion state of GNSs is defined as the GNS content above which the formation of a GNS-associated network is developed. Figure 3 shows the electrical conductivity (σ) of the PTT composites filled with GNS. The neat PTT had a measured conductivity of 1.8×10^{-17} S/cm. When the GNS content was increased in PTT/GNS composites, the GNSs came in contact with one another and gradually formed a conductive path. The PTT/GNS composites exhibited significantly improved conductivity and yielded a sharp transition from 0.29 to 1.17 vol %. At $\phi = 0.88$ vol %, σ became 5.32×10^{-5} S/cm, which was approximately three orders higher than the criterion ($\sim 10^{-8}$ S/cm) used for anti-static thin films.[13] The saturated conductivity of the PTT/GNS composites was 0.33 ± 0.23 S/cm with $\phi = 2.97$ vol %. Unlike neat PTT, a 15-order increase in σ was observed among the PTT/GNS composites, with $\phi = 1.77$ vol %. The percolation scaling law was applied to describe the association between σ and
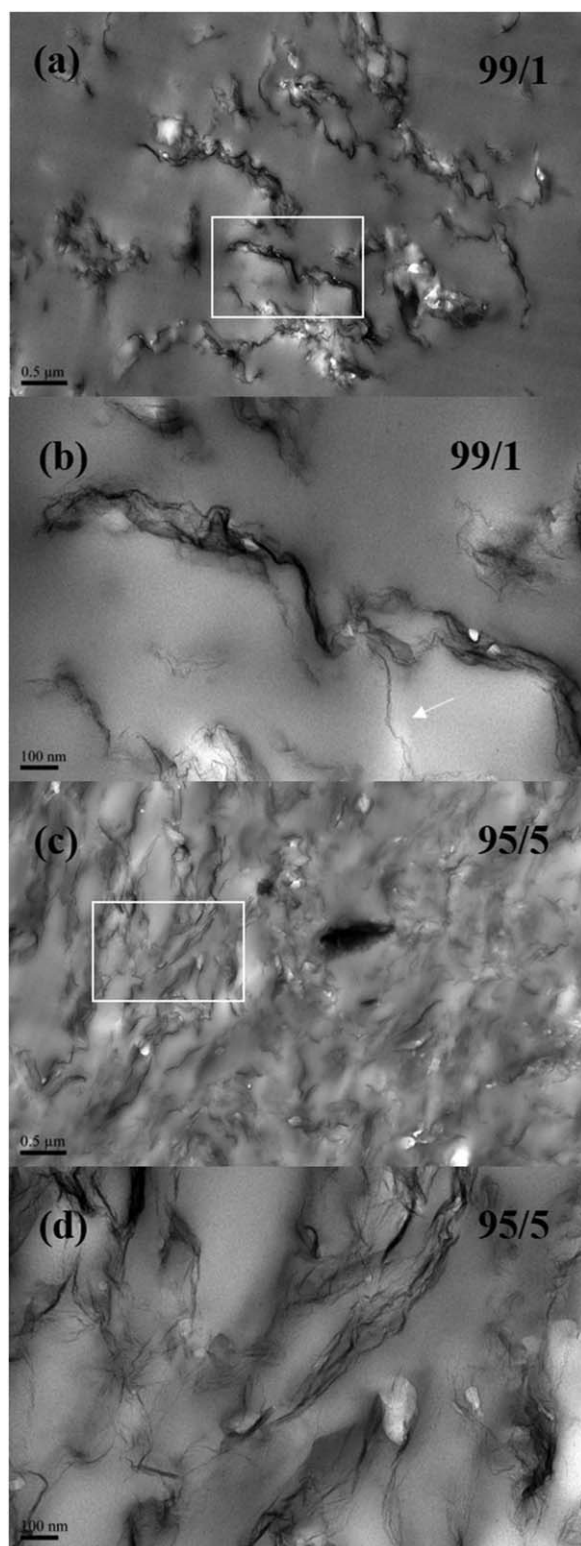
Figure 2. TEM images of (a), (b) PTT/GNS 99/1 composites, and (c), (d) PTT/GNS 95/5 composites. (b) and (d) show the enlarged TEM images of (a) and (c), respectively.

$\phi - \phi_c$ and quantitatively determine the minimum volume fraction of the GNSs required to develop the network for electron transportation. The corresponding plots are provided in the inset of

Figure 3. According to the regression analysis, the determined ϕ_c and exponent values were 0.53 vol % (0.9 wt %) and 4.63, respectively. The TEM and electrical conductivity results revealed a homogeneous dispersion of GNSs in the PTT matrix through coagulation method. Compared with those of other composites (0.1–3.39 vol %),[2,5,12,13,42–46] our derived ϕ_c for the PTT/GNS composites was within the minimum level. According to Li et al.[3], the ϕ_c of the PTT/GNS composites prepared by melt compounding range from 3 to 5 wt %. These values are higher than our results. Moreover, the σ value of the PTT/GNS composites with 2.97 vol % GNS was slightly higher than that of the poly(styrene-co-butyl acrylate)/GNS composites with 10 wt % GNS prepared via emulsion polymerization.[10] The simple coagulation process can obviously require small amount of GNSs in the same order σ for PTT/unmodified GNS composites. The ϕ_c value of the PTT/GNS composites in this work was higher than that of the PS/chemically modified GNSs prepared via coagulation method.[13] Nevertheless, The σ value of the PTT/GNS composites with 2.97 vol % GNS was higher than that of the PS/chemically modified GNS composites with 2.5 vol % GNS. These observations indicated that chemically modified GNS can enhance GNS–polymer interactions but the σ value of the polymer/chemically modified GNS composites became lower than that of the polymer/unmodified GNS composites. Moreover, the experimental ϕ_c value of the PTT/GNS composites approximated the theoretical values,[36] that is, 0.58 vol % for the fillers with aspect ratios of about 1/217. However, the experimental ϕ_c value of the PTT/GNS composites was slightly lower than the theoretical ϕ_c value. This discrepancy may be attributed to the wrinkled GNS, the GNS aspect ratio distribution, and the GNS dispersion status.[47] Huang et al.[47] studied PLLA/CNT composites and concluded that σ increases along the crystallinity of the PLLA composites with CNT concentrations lower than ϕ_c. However, the PTT lamellae could epitaxially grow on GNS surfaces (as discussed later). During solidification from the melt, the relative
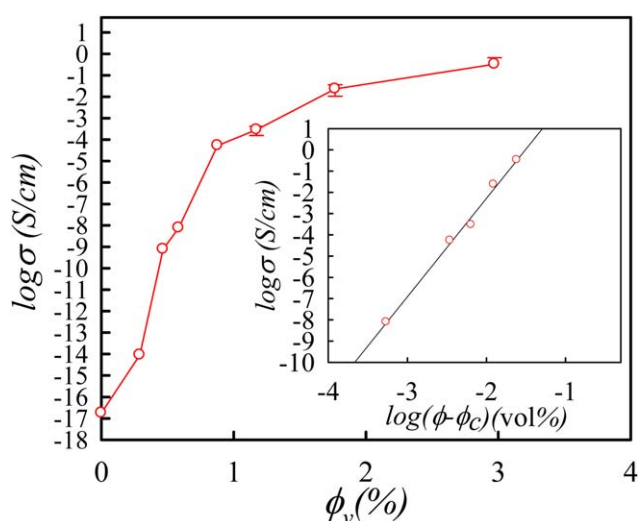

Figure 3. Conductivity versus GNS volume fraction of PTT/GNS composites. The inset shows the percolation scaling law between σ and $\phi - \phi_c$ for the composites. [Color figure can be viewed in the online issue, which is available at wileyonlinelibrary.com.]
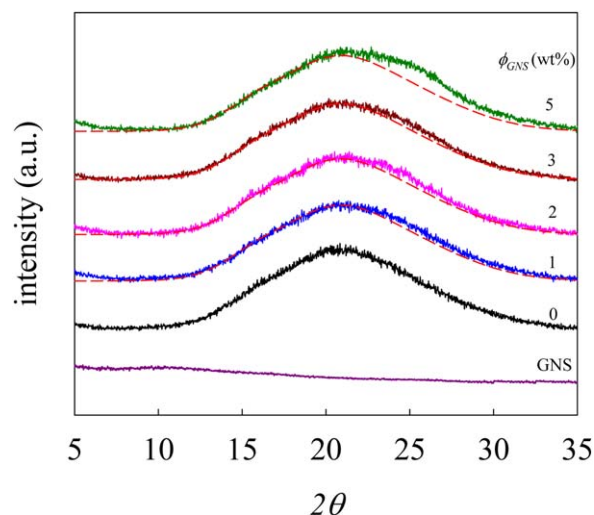
Figure 4. WAXD intensity profiles of melt-quenched PTT/GNS composites. The composites were held at 280 °C for 10 min, followed by quenching into liquid nitrogen. [Color figure can be viewed in the online issue, which is available at wileyonlinelibrary.com.]

position between GNS nanofillers could be gradually enlarged because of pronounced PTT crystal growth from GNS surfaces. These conditions are similar to our previous findings.[15,23] Therefore, in the current work, the σ value increased along with the GNS content as a result of the formation of a GNS–GNS network, and not because of the crystallinity of PTT matrix.

Non-Isothermal Crystallization of PTT/GNS Composites
To study the cold crystallization of PTT, the prepared composites were melted at 280 °C for 10 min and then subsequently quenched into liquid nitrogen to obtain the melt-quenched composites. Figure 4(a) shows the WAXD intensity profiles of the melt-quenched samples. The GNS only showed a new extensively broad halo at around $2\theta = 10°$, indicating that the graphene sheets of the GNSs were fully exfoliated. The WAXD intensity profiles of neat PTT showed a halo at $2\theta = 20.3°$ and full width at half-maximum = 10.8, which is consistent with the study of Chung et al.[48] A neat PTT sample showed an amorphous characteristic during such rapid cooling. When ϕ_{GNS} was 5 wt %, a diffraction hump at 22°–29° emerged. This outcome was in contrast to the behavior of the neat PTT samples that showed amorphous characteristics. The order structure is likely to be associated with the mesomorphic phase, which has been reported for PTT cold crystallization.[30] As shown in the WAXD results, the mesomorphic phase was formed during rapid cooling after the addition of GNS. Thus, GNSs can induce the order structure formation of the PTT chains. Given such results, the changes in GNS-filled PTT chain conformation during the subsequent cold crystallization should be analyzed.

Figure 5 shows the FTIR spectra of the neat PTT and PTT/GNS = 99/1 composite during stepwise heating to 225 °C. According to literatures,[49,50] the absorbance bands at 875 and 870 cm^{-1} are associated with the B$_{3u}$-CH out-of-plane bending of phenylene rings in the amorphous and crystalline phases, respectively. By contrast, the absorbance bands at 948 and 935 cm^{-1} are related to CH$_2$ rocking in a gauche conformation

in the crystalline phase. In the current work, the absorbance band, resulting from the trans-conformation was located at 815 and 978 cm^{-1}. Prior to heating, the neat PTT and PTT/GNS = 99/1 samples were completely amorphous, as indicated by the intensity of the WAXD and the amorphous band at 875 cm^{-1} (Figure 4). Upon heating, the neat PTT and PTT/GNS samples were gradually crystallized, as evidenced by the gradual absorbance increase in the 870, 935, and 948 cm^{-1} bands and the gradual absorbance decrease in the 815 and 978 cm^{-1} bands. These absorbance changes, which are consistent with previous findings on isothermal cold crystallization,[30] revealed the trans-to-gauche transition behavior in PTT cold crystallization.[51]

Figure 6 shows the normalized area of the 948 and 935 cm^{-1} bands and the variation in the absorbance peak at 875–870 cm^{-1} as a function of temperature for the neat PTT and its
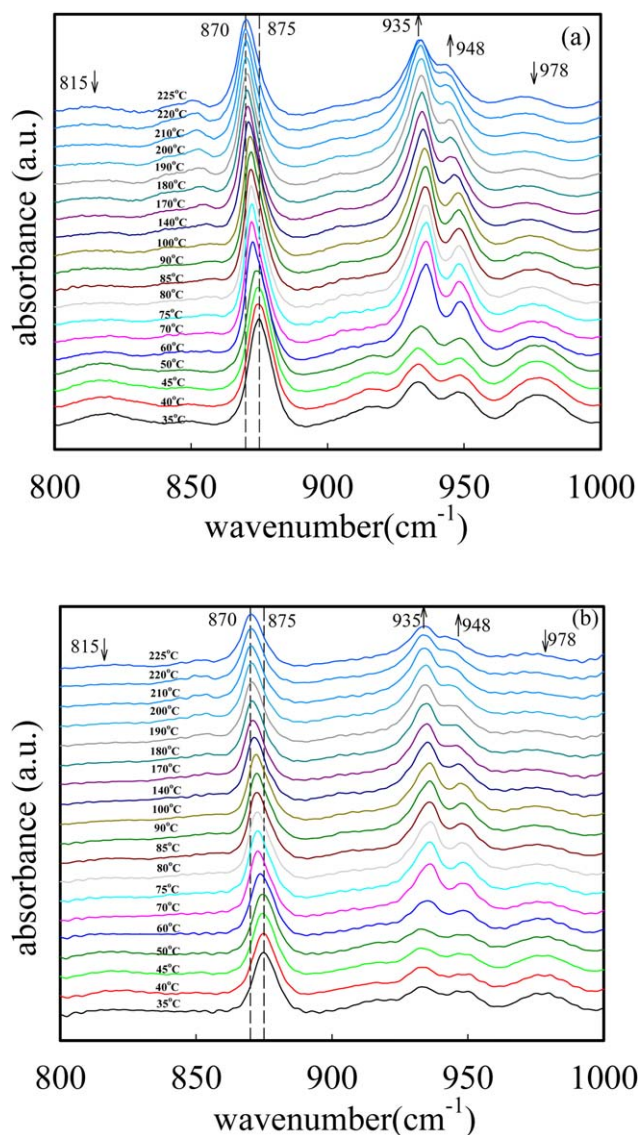

Figure 5. FTIR spectra of melt-quenched samples of (a) neat PTT, and (b) PTT/GNS = 99/1 during stepwise heating. [Color figure can be viewed in the online issue, which is available at wileyonlinelibrary.com.]
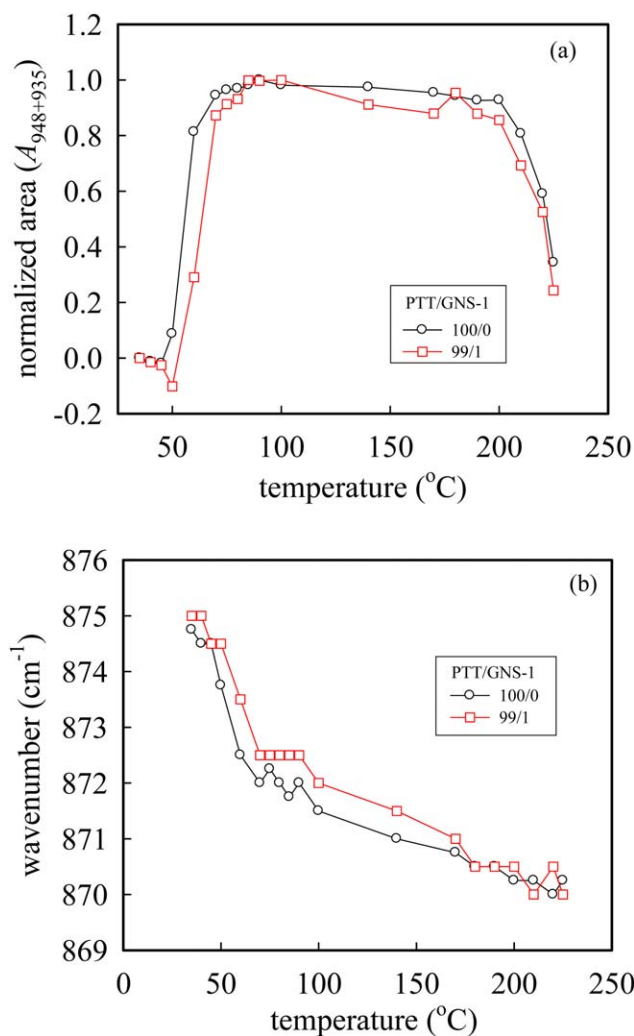
Figure 6. (a) Integrated area of the 1222 cm^{-1} band ($A_{948 + 935}$) and (b) variation in absorbance peak with temperature during stepwise heating. [Color figure can be viewed in the online issue, which is available at wileyonlinelibrary.com.]

GNS composites at 1 wt % GNS loading. The normalized area of the bands at 935 and 948 cm^{-1} was used in the following equation[25]:

$$A_{935+948} = \frac{A_T - A_{35}}{A_{max} - A_{35}} \quad (1)$$

where $A_{935 + 948}$ is the relative crystallinity of PTT, and A_{max} is the maximum area of the 935 and 948 cm^{-1} bands. A_T and A_{35} are the areas of the 935 and 948 cm^{-1} bands at different temperatures and at 35 °C, respectively. The cold crystallization process was characterized by the increased and normalized integrated area at the 935 and 948 cm^{-1} peak [Figure 6(a)], which was accompanied by a gradual band shift from 875 cm^{-1} to 870 cm^{-1} [Figure 6(b)]. Furthermore, a band shift was observed during heating at 870.25 cm^{-1} and prior to crystal melting at approximately 200 °C, at which spectral recording became infeasible because of sample flow. Notably, the $A_{935 + 948}$ value of the PTT/GNS = 99/1 composites at 50 °C was lower than that at 35
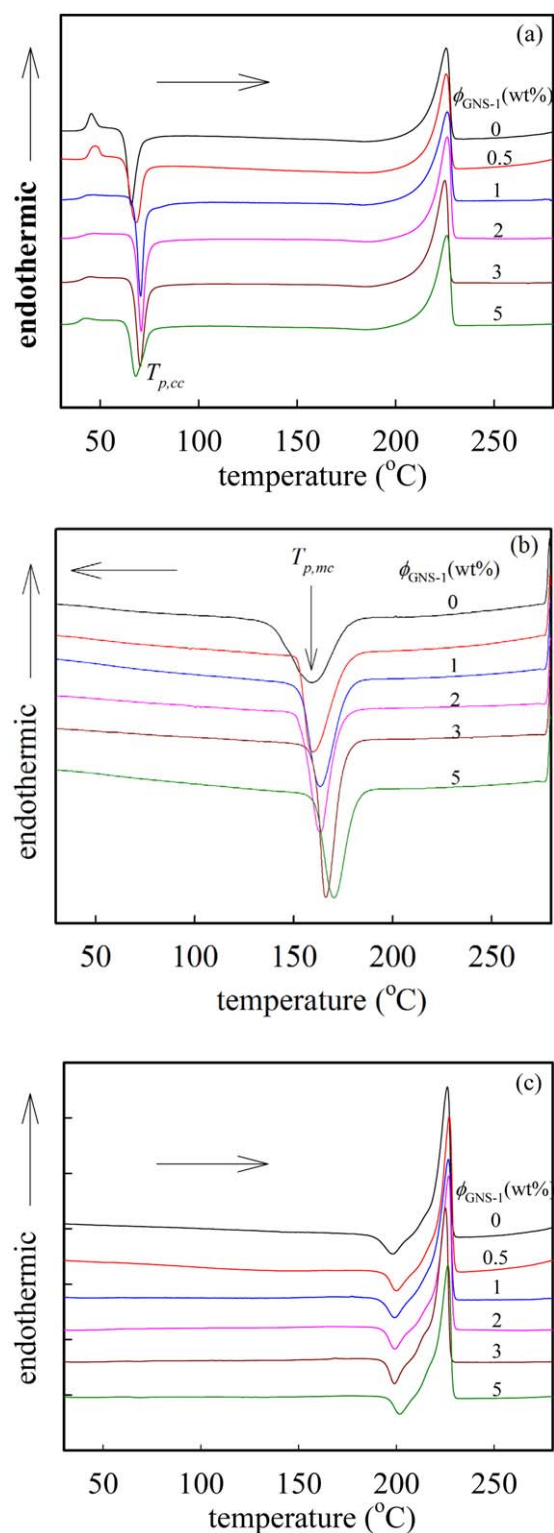

Figure 7. (a) DSC heating traces recorded for neat PTT and PTT/GNS composites for cold crystallization studies. The melt-quenched amorphous samples were heated at 10 °C/min to 280 °C. (b) DSC cooling for neat PTT and PTT/GNS composites for melt crystallization studies. After holding at 280 °C for 10 min, the samples were cooled at 10 °C/min to room temperature. (c) Subsequent heating at 10 °C/min after (b). [Color figure can be viewed in the online issue, which is available at wileyonlinelibrary.com.]

Table I. Thermal Properties of the PTT/GNS Composites Obtained from the Heating of Melt-Quenched Samples, and Cooling of the Melt after Holding at 280°C

PTT/GNS	T_g (°C)	$T_{p,cc}$ (°C)	$\Delta H_{cc}/(1-\phi_{GNS})$ (J/g)	$T_{m,f}$ (°C)	$T_{p,mc}$ (°C)	$t_{1/2}$ (min)	$\Delta H_{mc}/(1-\phi_{GNS})$ (J/g)	T_d (°C)
100/0	42.1	65.8	42.7	225.3	159.0	1.80	54.5	340.8
99.5/0.5	43.0	68.3	46.5	225.7	159.7	1.66	54.9	360.3
99/1	41.2 ± 0.1	70.4 ± 0.1	45.2	226.2	163.0 ± 0.6	1.35	57.8	367.0
98/2	40.9	70.8	43.2	226.2	163.3	0.93	55.4	358.9
97/3	41.4	70.3	45.6	225.0	166.3	0.91	57.5	363.4
95/5	39.3	68.0	41.4	226.0	170.3	1.08	52.1	367.5

°C. This result indicated that the gauche conformation of the PTT/GNS composites decreased at temperatures higher than the glass transition temperature (T_g). Due to the presence of GNSs, a few CH$_2$ segments of the PTT were induced to form a gauche conformation during rapid cooling but the moderate increase in regularity was not sufficient to cause the formation of crystalline structures. As a result, the chain structure of PTT was rearranged again after subsequent heating treatments. Moreover, the $A_{935 + 948}$ of the PTT/GNS = 99/1 composites at 60 °C was lower than that of the neat PTT at 60 °C. Meanwhile, the band between 875 and 870 cm^{-1} of the PTT/GNS = 99/1 composites was slightly higher than that of the neat PTT at the same temperature [Figure 6(b)]. These results also indicated that the cold crystallization of the PTT composites was retarded by the GNSs.

Figure 7(a) shows the DSC heating traces of the melt-quenched composites. T_g was determined from the mid-point of the heat-capacity jump, whereas the peak temperature of the cold crystallization was denoted as $T_{p,cc}$. Crystallization enthalpy, which was determined from the integral area of the exotherm, was represented by ΔH_{cc}. To represent the crystallizability of the PTT matrix in the presence of GNSs, ΔH_{cc} was normalized with the PTT content. The data are listed in Table I. T_g remained unchanged at approximately 41.7 °C with increased GNS content and then slightly decreased to 39.3 °C with a 5 wt % GNS content. The variation could be attributed to the improved heat conduction resulting from high GNS content.

$T_{p,cc}$ shifted to slightly high temperature with increased ϕ_{GNS}. By contrast, $T_{p,cc}$ slightly decreased with the reduction in PTT crystallizability when ϕ_{GNS} was >3%. When ϕ_{GNS} increased, the normalized ΔH_{cc} initially increased but subsequently decreased with increased ϕ_{GNS} because some mesomorphic phases already developed in the melt-quenched samples with high GNS loading prior to heating. Moreover, the melting temperature of the cold-crystallized composites was relatively unchanged, as shown in Figure 7(a). With regard to the kinetics of cold crystallization, consistent results were obtained between DSC and FTIR measurements.

To investigate melt crystallization, the samples were held at 280 °C for 10 min, followed by cooling at a rate of 10 °C/min. Figure 7(b) shows the cooling curves with a melt crystallization peak temperature and exothermic enthalpy, denoted as $T_{p,mc}$ and ΔH_{mc}, respectively. To represent the crystallizability of the PTT matrix in the presence of GNSs, ΔH_{mc} was also normalized

with the PTT content. The half crystallization time ($t_{1/2}$) of the PTT/GNS composites was used in the following equation[4]:

$$t_{1/2} = \frac{T_{on,mc} - T_{p,mc}}{X} \qquad (2)$$

where $T_{on,mc}$ was determined from the extrapolation of the melt-crystallization peak to the baseline, and X is the cooling rate (°C/min). These data are also listed in Table I. $T_{p,mc}$ continuously increased along with ϕ_{GNS}, and a maximum shift of 11.3 °C was obtained for the composites with ϕ_{GNS} of 5 wt %. Furthermore, as ϕ_{GNS} increased, $t_{1/2}$ initially decreased and then slightly increased, whereas the normalized ΔH_{mc} increased and subsequently decreased (Table I). These findings showed that the crystallizability of the PTT chains decreased at high ϕ_{GNS}. A subsequent heating scan of the melt-crystallized samples showed the melting of the PTT crystal [Figure 7(c)]. The melting temperature of the second heating was almost unchanged, whereas a small exothermic peak was observed before the melting peak. This finding indicated that a melting/recrystallization/re-melting event occurred during DSC heating scan for PTT/GNS composites, similar to the findings of Srimoaon et al.[52]

The samples were dynamically melt-crystallized at a cooling rate of 10 °C/min after being held at 280 °C for 10 min to study the effect of GNSs on PTT crystals during non-isothermal crystallization. Figure 8(a) shows the WAXD intensity profiles of the melt-crystallized PTT/GNS samples. The characteristic diffraction peaks of the PTT crystals[29,52] were observed at 2θ of 15.3°, 16.8°, 19.4°, 21.8°, 23.6°, 24.6°, and 27.3° for the PTT/GNS composite samples. Notably, the diffraction peak at 26°, which was associated with the d-spacing of the graphitic structure, was not detected for the PTT/GNS composites. Thus, GNSs might not have adhered again after composite preparation and might have been well-dispersed in the PTT composites. These TEM, electrical conductivity, and WAXD results demonstrated that the o-DCB-phenol was an effective dispersion medium for GNSs, similar to a previous report on PET/CNT composites.[16] After the deconvolution of the diffraction curves, crystallinity was estimated from the ratio of the integrated intensities from all the crystalline peaks to the total intensity curve. As shown in Figure 8(b), the PTT/GNS composites exhibited a maximum crystallinity of 50.3% for a ϕ_{GNS} of 2 wt %. The crystallinity decreased to 35% when ϕ_{GNS} was increased to 5 wt %. With the addition of the GNSs to PTT, the crystallinity and $t_{1/2}$ of the PTT/GNS composites decreased at high GNS content. This
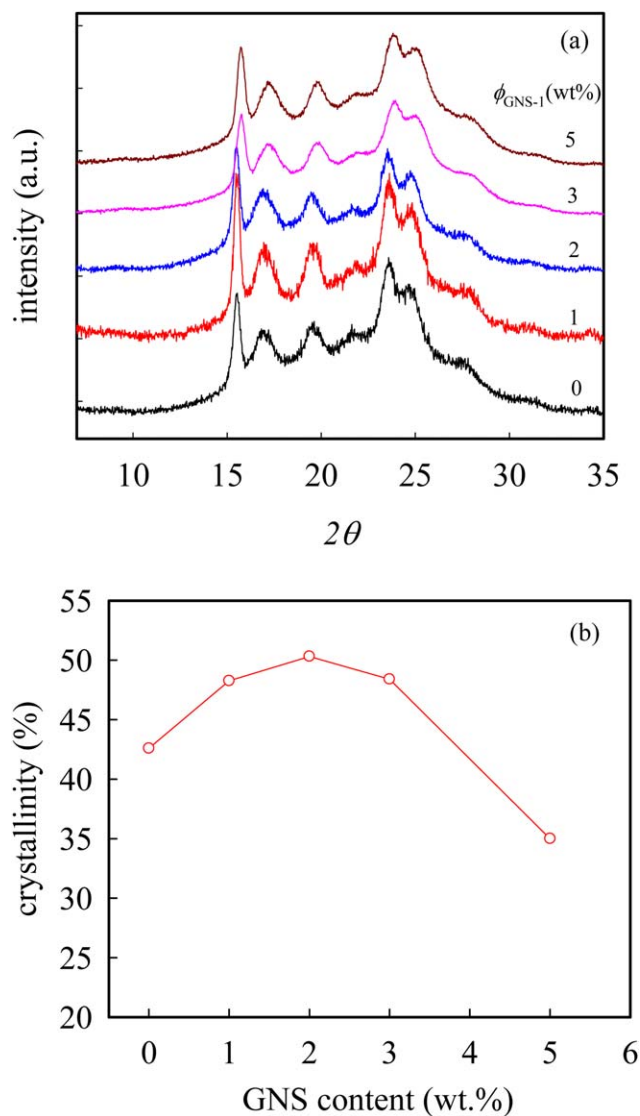
Figure 8. (a) WAXD intensity profiles and (b) crystallinity of the PTT/GNS composites melt-crystallized non-isothermally at cooling rate 10 °C/min. [Color figure can be viewed in the online issue, which is available at wileyonlinelibrary.com.]

the PTT and oxygen functional groups of GO would increase the crystallizability of the PTT chains. The increase in the magnitude of the $T_{p,mc}$ value of the PET/GNS composites was slightly higher than that of PTT/GNS composites given with the same filler contents.[4] PTT has similar a chemical composition to PET, and both are members of a linear aromatic polyester family. Although PTT has a relatively rapid crystallization rate relative to PET, the increase in the crystallizability of the PET chains is higher than that of the PTT chains with GNSs.

Lamellar Morphologies of PTT Composites

The morphological features of the PTT/GNS composites with non-isothermal crystallization at a cooling rate of 10 °C/min
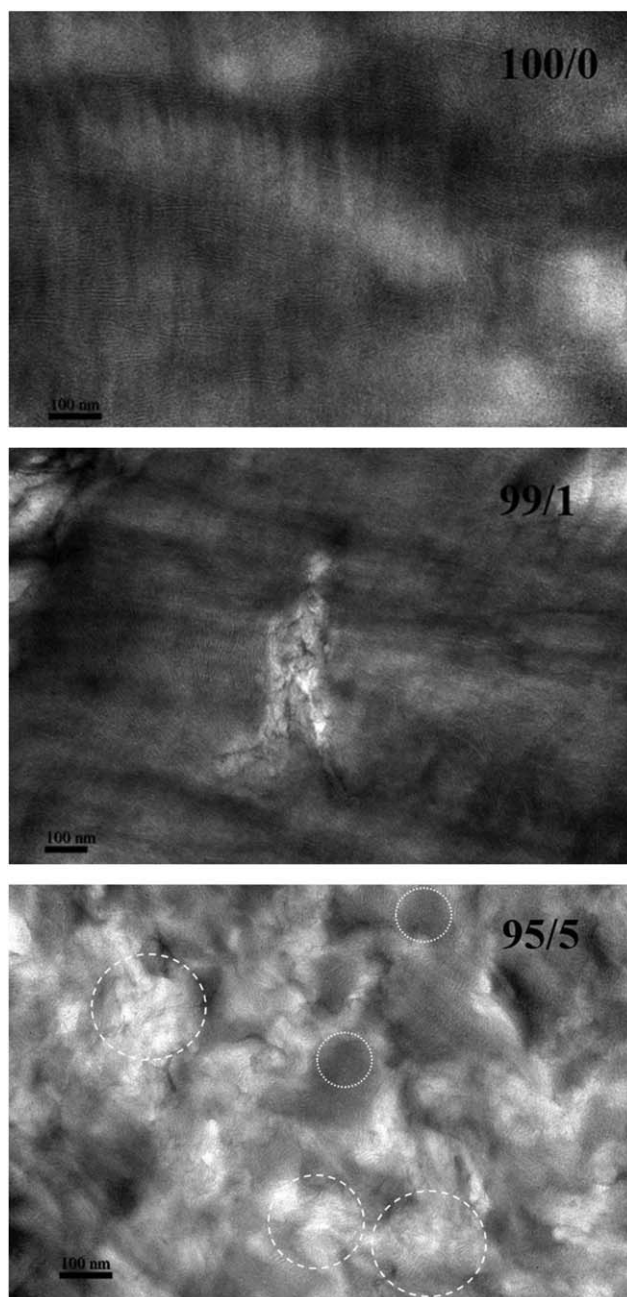

Figure 9. TEM images of the PTT/GNS composites.

finding agrees with the study of Aoyama *et al.*,[4] indicating the confinement effect in the PTT/GNS composites.

Compared with other PTT/GNS composites,[3] the PTT/GNS composites prepared by melt compounding exhibited a smaller increase in $T_{p,mc}$ given the same filler content. This difference indicates that the GNS dispersion state in the PTT matrix via coagulation was better than the dispersion state in the PTT matrix via melt compounding. Thus, PTT composites with good GNS dispersion state equated to the good opportunity to induce PTT nuclei. The increase in the $T_{p,mc}$ value of the PTT/GNS composites was smaller than that of the PTT/GO composites given the same filler contents.[33] According to FTIR results (Supporting Information, Figure S2), the number of the oxygen functional groups of GNS was extremely fewer than that of GO. This result indicated that the strong hydrogen bond between
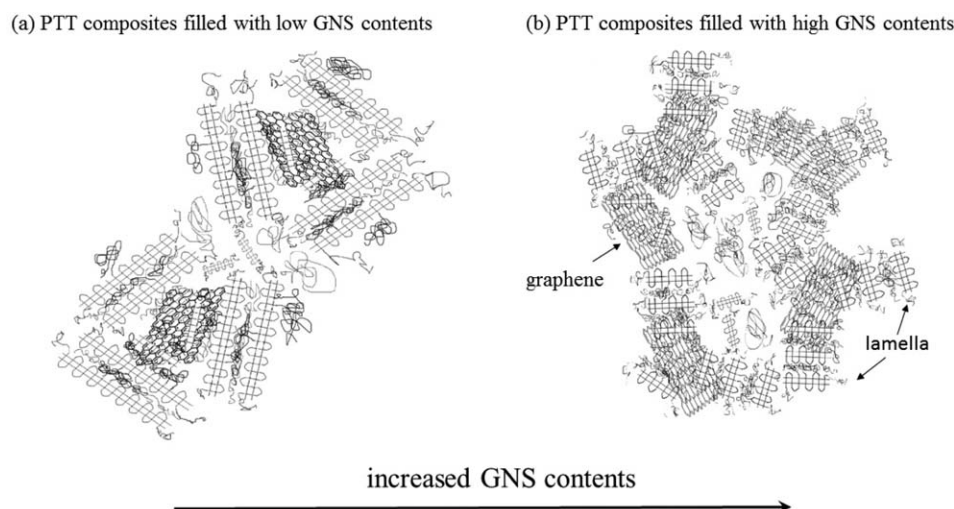
Figure 10. Schematic of the lamella morphology change of the PTT composites filled with various GNS contents.

were obtained by TEM (Figure 9). Edge-on PTT lamellae were observed as bright lines after the amorphous regions were preferentially stained with RuO_4 vapors, resulting in relatively darkened appearance. The neat PTT exhibited an ordered lamella morphology, which persisted qualitatively in the PTT/GNS = 99/1 composites. By contrast, high GNSs loadings (95/5) led to randomly oriented lamella stacks with reduced lateral dimensions. The dashed circles indicated that the edge-on lamellae epitaxially grew on top of the GNS. High-resolution TEM images are shown in Supporting Information, Figure S4. The result revealed that the heterogeneous nuclei of the PTT crystals were induced by GNS. The dotted circles indicated the amorphous region between lamella stacks; some amorphous regions could be readily observed at the impingement of the growing lamella stacks. For the PTT/GNS composites, the heterogeneous nuclei could arise from the bulk between GNSs or the epitaxial crystallization on the GNS surface. After high GNS loading, heterogeneous nucleation in the bulk between the GNSs became more difficult, and the GNS surface-induced nucleation eventually dominated. Some crystallizable PTT chains (or segments) may possibly be trapped in these lamella-free regions because of the confinement effect. The formation of a new lamella was challenging because of the constraints from the neighboring lamellae. Despite the restricted mobility resulting from the geometrical confinements, these trapped PTT chains (or segments) may undergo short-range motion to develop a less perfect crystallite similar to an aggregate of chains with a certain level of crystallographic packing in directions parallel and perpendicular to the chain axis. The average lamella thickness, l_c, was determined from a collection of about 200 lamella populations (Figure 9). The l_c values of the neat PTT, PTT/GNS = 99/1, and PTT/GNS = 95/5 were about 3.9 ± 0.4, 3.9 ± 0.6, and 3.9 ± 0.4 nm, respectively. Thus, l_c significantly remained unchanged regardless of ϕ_{GNS}.

GNSs are layer structures with a thickness of several nanometers and a lateral size of several micrometers. According to the FTIR results (Supporting Information, Figure S2), only weak hydrogen bond interactions existed between the PTT and GNS because of the insufficient number of oxygen functional groups on the GNS.

Moreover, a π–π interaction between the surface of the GNSs and the phenylene group of PTT was deemed possible. Thus, the GNSs absorbed fewer PTT chains though hydrogen bond interaction than through van der Waals force. The GNSs formed a GNS–GNS network path in the PTT composites as ϕ_{GNS} increased to 1 wt %, which was slightly higher than ϕ_c. Moreover, the distance between the GNS in the PTT composites could decrease and subsequently aggregate with increased ϕ_{GNS}. By contrast, the PTT chain was further constrained in the GNS–GNS network. During cooling, profound PTT nuclei were randomly developed on the GNS surface to form the lamellae (Figure 10). Overgrown lamellae from the GNS surface of the PTT composites filled with high ϕ_{GNS} resulted in the retardation of regular PTT crystalline lamellae growth in the GNS–GNS network area. However, the lateral dimension of the lamella developed in the bulk between the GNS–GNS network decreased and formed the amorphous region between the lamella stacks. The PTT composites filled with GNSs featured enhanced PTT crystallization rate. However, this process could retard crystalline lamellae growth and result in decreased PTT crystallinity, as verified during melt-crystallization at high ϕ_{GNS}.

Isothermal Crystallization and Crystal Melting

For non-isothermal crystallization and lamellar morphologies of PTT/GNS composites, competition exists between nucleation and confinement effects during PTT/GNS composites crystallization with high GNS content. Therefore, this study focused on the isothermal crystallization dynamics of PTT/GNS composites with high GNS content. Based on the time variation of the crystallization isotherms and relative crystallinity of the GNS-filled PTT composites at 194 °C (Supporting Information, Figure S3), the Avrami equation was applied to describe the kinetics of isothermal crystallization[23,53]:

$$1 - X(t) = \exp\left[-k(t - t_i)^n\right] \tag{3}$$

where $X(t)$ is the relative crystallinity; t_i and t are the induction and crystallization times, respectively; n is the Avrami exponent; and k is the overall crystallization rate. Based on eq. (3), the initial slope corresponding to exponent n and the value of k can be deduced from the intercept by plotting $\ln[-\ln\{1 - X(t)\}]$
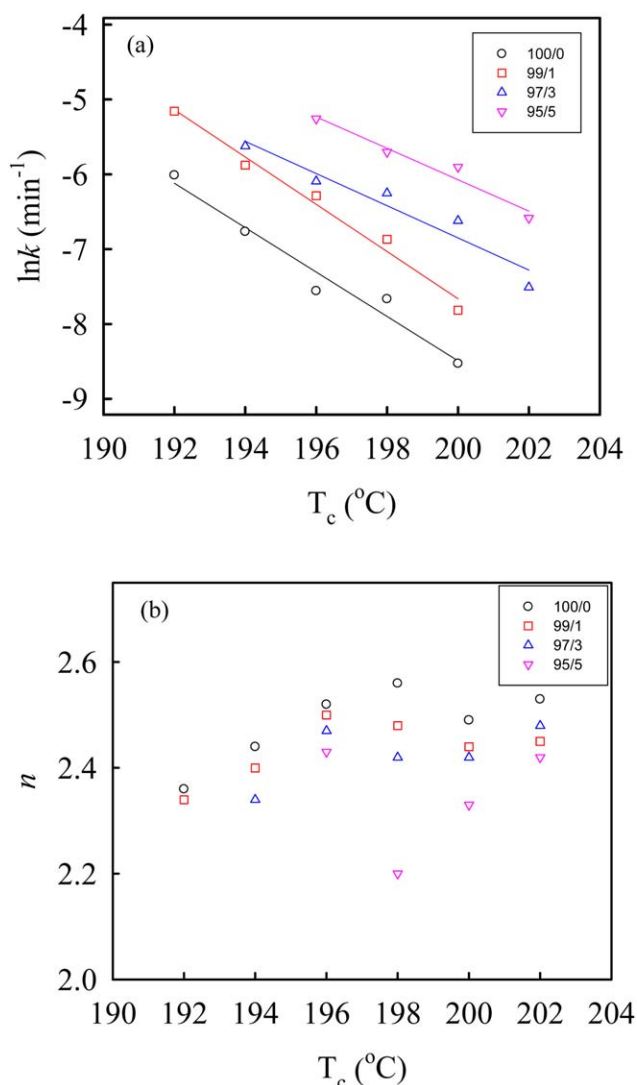
Figure 11. Effects of crystallization temperature on (a) overall crystallization rate, k, (b) Avrami exponent, n. [Color figure can be viewed in the online issue, which is available at wileyonlinelibrary.com.]

versus $\ln(t - t_i)$ (Supporting Information, Figure S3). Figure 11 shows the derived values of k and n for the PTT/GNS composites at different T_c values. As expected, the crystallization rate at a high T_c decreased for all the samples. At a given T_c, addition of GNS increased PTT crystallization. An increase in k by an order of magnitude was observed among the 3 wt % GNS at 200 °C. Moreover, the PTT/GNS composites with 5 wt % GNS featured higher k than those with 3 wt % GNS at a given T_c. This result indicated that the influence of nucleation effect on the overall crystallization rate is stronger than the influence of confinement. Notably, the derived Avrami exponent slightly decreased from a higher values ($\sim$2.5) for the neat PTT to a lower value ($\sim$2.4) for those with GNS contents [Figure 11(b)]. The Avrami exponent of the PTT/GNS composites ($\sim$2.4) suggested a heterogeneous nucleation together with 3D growth. By studying the melt crystallization of the sPS/GNS composites, Wang et al.[24] demonstrated that the Avrami exponent varies from 2.8 for the neat sPS to 2.5 and 1.5 for sPS/GNS = 95/5

composites with different GNS thickness of 2 and 50 nm, respectively; a tremendous increase in k was also observed. For the PLLA/GNS composites,[26] k initially increased and then subsequently decreased with the increase in GNS loading; however, the Avrami exponent changed irrespectively. Guo et al.[33] found that the Avrami exponent of the PTT/GO composites practically remained unchanged despite the GO loading.

The melting behavior of the isothermally crystallized composites was also studied in the current work. Figure 12(a) shows the results of the PTT/GNS = 95/5 composites crystallized at various T_c. Three melting peaks denoted by T_a, T_{ml}, and T_{mh} from low to high temperatures were detected for the samples crystallized at 192 °C. Multiple melting behaviors did not result from the PTT polymorphism because the PTT crystals exhibited only one modification during melt crystallization. T_{ml} gradually increased along with T_c, but T_{mh} was independent of T_c. T_a was always observed to be immediately above T_c, and such condition became increasingly evident at high T_c. Similar T_c effects on melting behavior were observed in the sPS/GNS composites with different values of ϕ_{GNS}.[24] The appearance of T_a was relatively obscure for the composites with low ϕ_{GNS}, and a barely visible T_a was detected for the neat PTT sample. The equilibrium melting temperature, T_m^o, is the most important parameter for a crystallizable polymer because crystallization kinetics depends on the supercooling degree, ΔT, which is defined by $T_m^o - T_c$. The classical Hoffman–Weeks approach was applied to determine T_m^o. By plotting the observed T_m as a function of T_c, the linear extrapolation with the $T_m = T_c$ line yielded the value of T_m^o. Figure 12(b) shows the T_c-dependence of the melting peak temperatures for the PTT/GNS composites. Regardless of the GNS content, all the composites showed a superposition of the measured T_a, T_{ml}, and T_{mh}. These findings suggested that GNS addition had no influence on the crystalline lamellae melting. Moreover, the lamella thickness remained intact. Based on the T_{ml} data, the determined T_m^o was approximately 244.4 °C for both the neat PTT and the GNS-filled composites. Our derived T_m^o for the PTT was within the intermediate range compared with those of other studies (237 °C–252 °C).[48,54–56] As shown in Figure 12(b), a linear line with a slope of unity was observed between T_a and T_c, and T_a was always 9.6 °C $\pm$ 1.4 °C above T_c. The presence of the annealing peak has been described in detail for certain semi-stiff polymers such as PTT,[56,57] PET,[58] and iPS.[59] One hypothesis for T_a is ascribed to the presence of a rigid amorphous phase between the mobile amorphous and crystalline lamella phases. The formation of a rigid amorphous phase cannot be absolutely excluded; however, another plausible source is the melting of the imperfect microcrystallites that develop between the main lamella stacks. After the addition of GNS, rapid nucleation reduced the number of lamellae in each lamella stack. Moreover, certain amorphous regions were formed at the impingement of the growing lamella stacks. Similar to the findings of a study on the melting process of PE with sufficient branching content,[60] an annealing peak was observed and considered to be caused by the formation of fringed-micelles or chain cluster structures developed in the constrained environments between the lamellae.
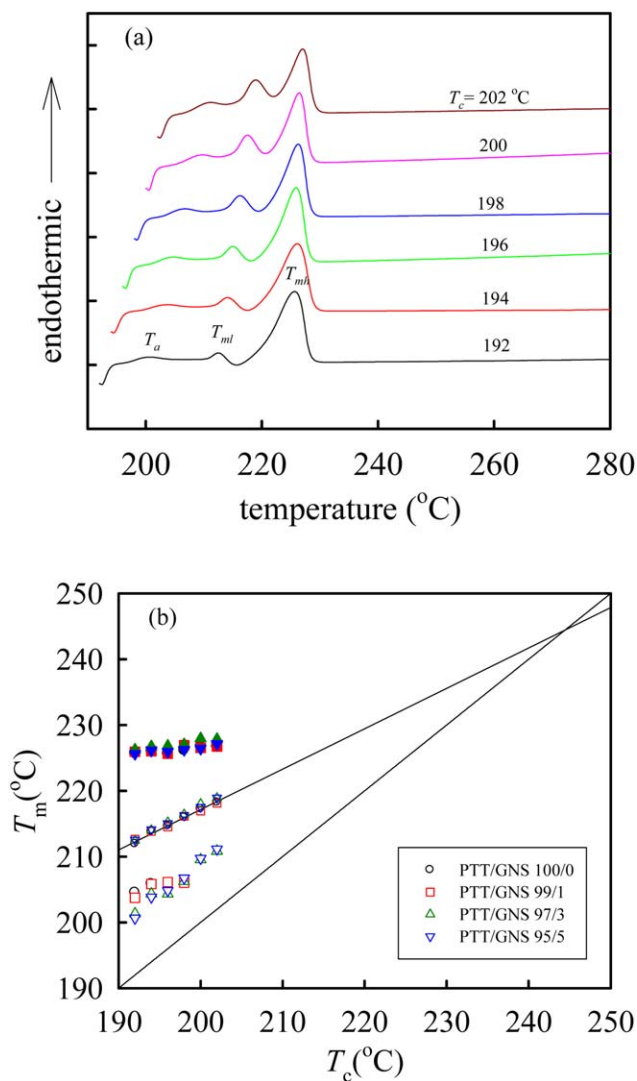
with the PTT/GO composite morphologies.[33] However, unlike other GNS-filled polymer composites, such as sPS[24] and PE,[19] the total nucleation sites of spherulite did not increase enough to disrupt the growth of spherulites in the GNS-filled PTT composites. Therefore, the growth mechanism of PTT spherulite did not change in the PTT/GNS composites.

TGA was performed on the composites to investigate the effect of GNSs on the thermal stability of the PTT matrix. The resulting curves are shown in Figure 14. For the composites, the weights that remained at 500 °C were almost entirely caused by
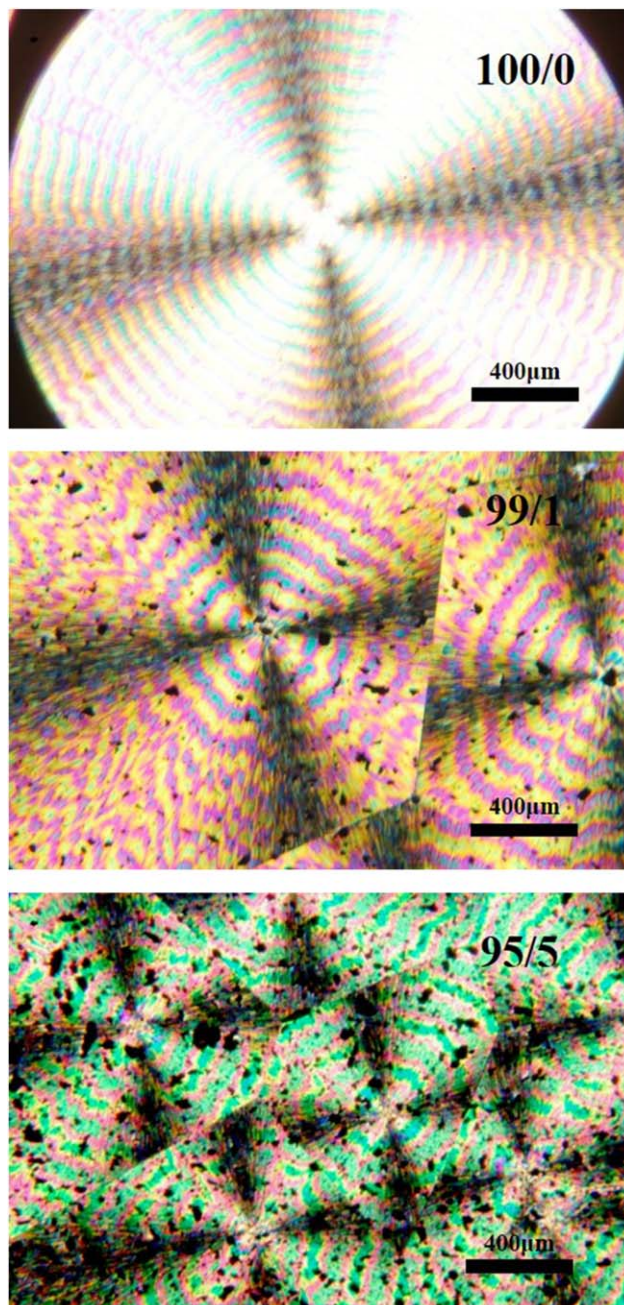

Figure 12. (a) Melting behavior of PTT/GNS = 95/5 composites crystallized isothermally at various T_c, (b) Determination of equilibrium melting temperature of the PTT/GNS composites by Hoffman–Weeks plot. (*Filled symbols* for T_{mh}, open symbols for T_{ml}, and *open symbols* with a *dot center* for T_a.). [Color figure can be viewed in the online issue, which is available at wileyonlinelibrary.com.]

Figure 13 shows the PLM images of the samples crystallized at 196 °C. According to the study of Hong *et al.*,[61] 196 °C is at regime II of the secondary nucleation theory. A pronounced decrease in the size of PTT banded spherulites was observed. For composites with 1 wt % GNS, spherulites were still identified; however, their diameter and banded structures were significantly small and irregular, respectively. Nucleation density increased as ϕ_{GNS} increased to 5 wt %; however, spherulites were still identified. This finding demonstrated the nucleation ability of the GNSs, which was consistent with the derived Avrami exponent (~2.4), thereby suggesting a heterogeneous nucleation together with 3D growth. The morphology observed by PLM suggested that heterogeneous nucleation was the dominant mechanism for PTT crystallization. Moreover, the addition of GNSs significantly increased the nucleation density in the composites, consistent

Figure 13. PLM images of the PTT/GNS composites crystallized at 196 °C. The scale bar is 400 μm. [Color figure can be viewed in the online issue, which is available at wileyonlinelibrary.com.]
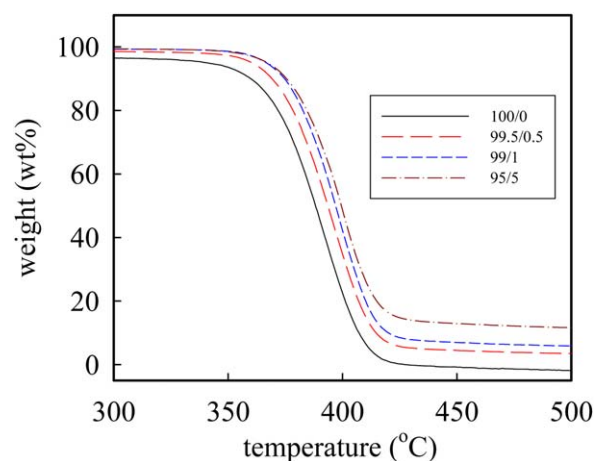
Figure 14. TGA curves of the PTT/GNS composites. [Color figure can be viewed in the online issue, which is available at wileyonlinelibrary.com.]

the remaining GNS. The T_d values were determined from the curves and displayed in Table I. The retardation of PTT decomposition was evident because of the presence of GNSs, and a maximum increase of 26.7 °C in T_d was observed for the 5 wt % GNS composites. The retardation was likely the result of adsorption by the activated GNS surface of the free radicals generated during PTT decomposition. The T_d of the PTT/GNS composites was smaller than that of the PTT/GO composites[33] with the same filler contents. This result could be attributed to the different processing methods for PTT/GNS and PTT/GO composites. Moreover, PTT/GO composites did not show a clear retardation of PTT decomposition during heating.

CONCLUSIONS

A coagulation method was used to prepare PTT composites filled with well-dispersed GNSs having o-DCB-phenol serving as solvent for solution blending. The method was effective, as indicated by the low electrical threshold of 0.53 vol %. Regardless of GNS content, the glass transition and equilibrium melting temperature of the PTT matrix remained unchanged at 41.7 °C and 244.4 °C, respectively. In the case wherein liquid nitrogen was used to quench the melt, a PTT mesomorphic phase was formed despite the extremely short crystallization time with high GNS loading. For PTT/GNS composites melt crystallization, the epitaxially grown lamellae on top of the GNS were observed by TEM. The PTT banded spherulites were still identified by PLM in the PTT/GNS composites with high GNS loading. According to the results of the non-isothermal and isothermal crystallizations, the PTT crystallization rate increased with GNS content. The enhanced crystallization rate was attributed to the numerous nucleation sites provided by the GNSs. This finding resulted in PTT crystal epitaxial growth on the GNS surface. By contrast, the crystallinity and half crystallization time for non-isothermal crystallization at high GNS content were influenced by the confinement effect. Therefore, the PTT crystallinity initially increased with GNS loading. However, crystallinity reached its maximum value near the electrical percolation threshold and then subsequently decreased with the increase in GNS content. This result was attributed to the over-

grown lamellae on the GNS surface of the PTT composites with high GNS content. This condition led to the retardation of the regular PTT crystalline lamellae growth in the GNS–GNS network area. GNSs promote thermal stability of PTT composites at high temperatures.

ACKNOWLEDGMENTS

REFERENCES

1. Novoselov, K. S.; Geim, A. K.; Morozov, S.; Jiang, D.; Zhang, Y.; Dubonos, S.; Grigorieva, I.; Firsov, A. *Science* **2004**, *306*, 666.

2. Zhang, H. B.; Zheng, W. G.; Yan, Q.; Yang, Y.; Wang, J. W.; Lu, Z. H.; Ji, G. Y.; Yu, Z. Z. *Polymer* **2010**, *51*, 1191.

3. Li, M.; Jeong, Y. G. *Macromol. Mater. Eng.* **2011**, *296*, 159.

4. Aoyama, S.; Park, Y. T.; Ougizawa, T.; Macosko, C. W. *Polymer* **2014**, *55*, 2077.

5. Chen, G.; Weng, W.; Wu, D.; Wu, C. *Eur. Polym. J.* **2003**, *39*, 2329.

6. Reddy, K. R.; Sin, B. C.; Ryu, K. S.; Kim, J. C.; Chung, H.; Lee, Y. *Synth. Met.* **2009**, *159*, 595.

7. Reddy, K. R.; Sin, B. C.; Yoo, C. H.; Sohn, D.; Lee, Y. *J. Colloid Interface Sci.* **2009**, *340*, 160.

8. Hassan, M.; Reddy, K. R.; Haque, E.; Minett, A. I.; Gomes, V. G. *J. Colloid Interface Sci.* **2013**, *410*, 43.

9. Hassan, M.; Reddy, K. R.; Haque, E.; Faisal, S. N.; Ghasemi, S.; I Minett, A.; Gomes, V. G. *Compos. Sci. Technol.* **2014**, *98*, 1.

10. Park, N.; Lee, J.; Min, H.; Park, Y. D.; Lee, H. S. *Polymer* **2014**, *55*, 5088.

11. Moradi, M.; Mohandesi, J. A.; Haghshenas, D. F. *Polymer* **2015**, *60*, 207.

12. Zhang, H. B.; Zheng, W. G.; Yan, Q.; Jiang, Z. G.; Yu, Z. Z. *Carbon* **2012**, *50*, 5117.

13. Stankovich, S.; Dikin, D. A.; Dommett, G. H.; Kohlhaas, K. M.; Zimney, E. J.; Stach, E. A.; Piner, R. D.; Nguyen, S. T.; Ruoff, R. S. *Nature* **2006**, *442*, 282.

14. Shen, J. W.; Chen, X. M.; Huang, W. Y. *J. Appl. Polym. Sci.* **2003**, *88*, 1864.

15. Huang, C. L.; Wang, C. *Carbon* **2011**, *49*, 2334.

16. Hu, G.; Zhao, C.; Zhang, S.; Yang, M.; Wang, Z. *Polymer* **2006**, *47*, 480.

17. Potts, J. R.; Dreyer, D. R.; Bielawski, C. W.; Ruoff, R. S. *Polymer* **2011**, *52*, 5.

18. Wang, C.; Chiu, Y. C.; Huang, C. L. *Mater. Chem. Phys.* **2015**, *164*, 206.

19. Cheng, S.; Chen, X.; Hsuan, Y. G.; Li, C. Y. *Macromolecules* **2012**, *45*, 993.

20. Li, L.; Li, C. Y.; Ni, C. *J. Am. Chem. Soc.* **2006**, *128*, 1692.

21. Lu, K.; Grossiord, N.; Koning, C. E.; Miltner, H. E.; Mele, B.; Loos, J. *Macromolecules* **2008**, *41*, 8081.

22. Song, P.; Cao, Z.; Cai, Y.; Zhao, L.; Fang, Z.; Fu, S. *Polymer* **2011**, *52*, 4001.

23. Huang, C. L.; Wang, C. *Eur. Polym. J.* **2011**, *47*, 2087.

24. Wang, C.; Chiu, Y. C. *J. Polym. Res.* **2015**, *22*, 76.

25. Xu, J. Z.; Chen, T.; Yang, C. L.; Li, Z. M.; Mao, Y. M.; Zeng, B. Q.; Hsiao, B. S. *Macromolecules* **2010**, *43*, 5000.

26. Xin, S.; Li, Y.; Zhao, H.; Bian, Y.; Li, W.; Han, C.; Dong, Q.; Ning, Z.; Dong, L. *J. Therm. Anal. Calorim.* **2015**, *122*, 379.

27. Wu, D.; Yang, T.; Sun, Y.; Shi, T.; Zhou, W.; Zhang, M. *Polym. Int.* **2011**, *60*, 1497.

28. Ning, N.; Fu, S.; Zhang, W.; Chen, F.; Wang, K.; Deng, H.; Zhang, Q.; Fu, Q. *Prog. Polym. Sci.* **2012**, *37*, 1425.

29. Ho, R. M.; Ke, K. Z.; Chen, M. *Macromolecules* **2000**, *33*, 7529.

30. Chuang, W. T.; Su, W. B.; Jeng, U. S.; Hong, P. D.; Su, C. J.; Su, C. H.; Huang, Y. C.; Laio, K. F.; Su, A. C. *Macromolecules* **2011**, *44*, 1140.

31. Xu, Y.; Jia, H. B.; Piao, J. N.; Ye, S. R.; Huang, J. *J. Mater. Sci.* **2008**, *43*, 417.

32. Paszkiewicz, S.; Pawelec, I.; Szymczyk, A.; Špitalský, Z.; Mosnáček, J.; Kochmańska, A.; Rosłaniec, Z. *Polym. Eng. Sci.* **2015**, *55*, 2222.

33. Guo, C.; Ji, L.; Li, Y.; Yang, X.; Tu, Y. *J. Appl. Polym. Sci.* **2014**, *131*, 40332.

34. Chuah, H.; Lin-Vien, D.; Soni, U. *Polymer* **2001**, *42*, 7137.

35. Gupta, A.; Choudhary, V. *Compos. Sci. Technol.* **2011**, *71*, 1563.

36. Garboczi, E.; Snyder, K.; Douglas, J.; Thorpe, M. *Phys. Rev. E* **1995**, *52*, 819.

37. Fuente, E.; Menendez, J.; Diez, M.; Suarez, D.; Montes-Moran, M. *J. Phys. Chem. B* **2003**, *107*, 6350.

38. Fernandez-Merino, M.; Guardia, L.; Paredes, J.; Villar-Rodil, S.; Solis-Fernandez, P.; Martinez-Alonso, A.; Tascon, J. *J. Phys. Chem. C* **2010**, *114*, 6426.

39. Ren, P. G.; Yan, D. X.; Ji, X.; Chen, T.; Li, Z. M. *Nanotechnology* **2011**, *22*, 055705.

40. Huang, C. L.; Peng, S. Y.; Wang, Y. J.; Chen, W. C.; Lin, J. H. *J. Appl. Polym. Sci.* **2015**, *132*, 41891.

41. Li, Q.; Li, Z.; Chen, M.; Fang, Y. *Nano Lett.* **2009**, *9*, 2129.

42. Qi, X. Y.; Yan, D.; Jiang, Z.; Cao, Y. K.; Yu, Z. Z.; Yavari, F.; Koratkar, N. *ACS Appl. Mater. Interfaces* **2011**, *3*, 3130.

43. Zhang, M.; Li, D. J.; Wu, D. F.; Yan, C. H.; Lu, P.; Qiu, G. M. *J. Appl. Polym. Sci.* **2008**, *108*, 1482.

44. Fan, P.; Wang, L.; Yang, J.; Chen, F.; Zhong, M. *Nanotechnology* **2012**, *23*, 365702.

45. Yoonessi, M.; Gaier, J. R. *ACS Nano* **2010**, *4*, 7211.

46. Tang, Z.; Kang, H.; Shen, Z.; Guo, B.; Zhang, L.; Jia, D. *Macromolecules* **2012**, *45*, 3444.

47. Huang, C.; Bai, H.; Xiu, H.; Zhang, Q.; Fu, Q. *Compos. Sci. Technol.* **2014**, *102*, 20.

48. Chung, W. T.; Yeh, W. J.; Hong, P. D. *J. Appl. Polym. Sci.* **2002**, *83*, 2426.

49. Ward, I.; Wilding, M. *Polymer* **1977**, *18*, 327.

50. Kim, K.; Bae, J.; Kim, Y. *Polymer* **2001**, *42*, 1023.

51. Poulin-Dandurand, S.; Pérez, S.; Revol, J. F.; Brisse, F. *Polymer* **1979**, *20*, 419.

52. Srimoaon, P.; Dangseeyun, N.; Supaphol, P. *Eur. Polym. J.* **2004**, *40*, 599.

53. Sperling, L. H. Introduction to Physical Polymer Science; John Wiley & Sons: New York, **2001**.

54. Huang, J. M.; Chang, F. C. *J. Polym. Sci. Part B: Polym. Phys.* **2000**, *38*, 934.

55. Wu, P. L.; Woo, E. M. *J. Polym. Sci. Part B: Polym. Phys.* **2002**, *40*, 1571.

56. Pyda, M.; Boller, A.; Grebowicz, J.; Chuah, H.; Lebedev, B.; Wunderlich, B. *J. Polym. Sci. Part B: Polym. Phys.* **1998**, *36*, 2499.

57. Sanz, A.; Nogales, A.; Ezquerra, T. A.; Soccio, M.; Munari, A.; Lotti, N. *Macromolecules* **2010**, *43*, 671.

58. Lee, Y.; Porter, R. S. *Macromolecules* **1987**, *20*, 1336.

59. Xu, H.; Ince, B. S.; Cebe, P. *J. Polym. Sci. Part B: Polym. Phys.* **2003**, *41*, 3026.

60. Alizadeh, A.; Richardson, L.; Xu, J.; McCartney, S.; Marand, H.; Cheung, Y.; Chum, S. *Macromolecules* **1999**, *32*, 6221.

61. Hong, P. D.; Chung, W. T.; Hsu, C. F. *Polymer* **2002**, *43*, 3335.